Forces and Flow Visualization of a Three-Dimensional Flapping Foil

Karl McLetchie, Melissa Flores, Franz Hover, Alexandra Techet, and Michael Triantafyllou
Department of Ocean Engineering
MIT, Cambridge, MA 02134
Email: kmwm@mit.edu

***Abstract*— Recent experimental and numerical work with unsteady flapping foil propulsors has shown that they are emerging as an efficient, high thrust alternative to traditional propulsors. In this paper, experimental force measurements for a three-dimensional flapping foil are presented, along with preliminary flow visualization data.**

The force measurements of thrust and lift were made with a flapping foil module that actuates a foil in a sinusoidal pitch and roll motion, similar to the motion of a penguin's wing. During symmetric flapping, a significant thrust force is produced that increases dramatically with Strouhal number. A maximum thrust coefficient, within the parameters allowed by the module, of Ct = 2.0 occurs at a Strouhal number of 0.8 and a peak angle of attack of 40 degrees.

During flapping in which the pitch angle is biased by a static angle, a mean lift coefficient is produced. A maximum mean lift coefficient of 3.5 was measured.

Flow visualization data were taken with a digital particle image velocimetry (DPIV) system. The images show that three large vortices are shed during each cycle of motion. Force calculations from this data will give the spanwise force distribution on the foil.

The results from this investigation into the performance of three-dimensional flapping foils will be applied directly to the development of flapping foil vehicles.

I. Introduction

Past investigations into flapping foil propulsion have been limited to two-dimensional flapping foils and simple drag based three-dimensional flapping foils.

Read [1] did experiments to investigate the propulsion and maneuvering forces produced by two-dimensional sinusoidally oscillating foils i.e, a rectangular planform heaving transverse to the flow and pitching. He measured thrust and lift forces over a parameter space of heave amplitudes, pitch amplitudes, and oscillation frequencies. He recorded planform area normalized thrust coefficients of 2.4 and efficiencies of up to 71.5%. He also investigated mechanisms to produce mean lift and showed that high mean lift coefficients could be achieved by adding a static bias to the foil pitch. Mean lift coefficients of over 4 were achieved in this manner.

Kato [2] has built two generations of underwater vehicles that use three-dimensional flapping foil propulsion. The foils on his vehicles use a drag based, "rowing", form of propulsion, instead of the lift based propulsion that this paper investigates.

A large body of work has been done on calculating forces from the flow around oscillating cylinders and two-dimensinal flapping foils [3] [4] [5]. Using DPIV images for these calculations is difficult because the DPIV camera can only capture a small part of the flow.

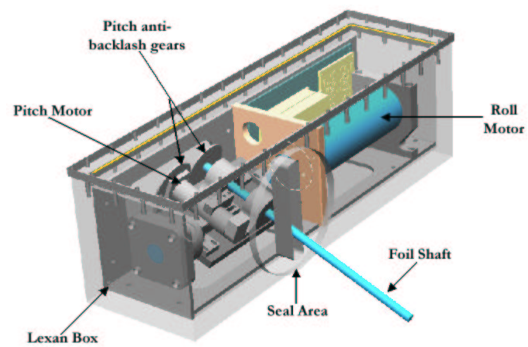

Fig. 1. solid model drawing of the flapping foil actuator

Lin and Rockwell were successful with calculating forces using Lighthill's moment of vorticity equation because they analyzed the flow around a cylinder started from rest with no ambient flow. Using this technique, they took their DPIV data before any vorticity had convected out of the images [6]. Their technique will not work with a flapping foil in a steady uniform flow.

Anderson [7] performed DPIV on a two-dimensional flapping foil to both understand the vortex wake of a flapping foil and to calculate the forces on the foil. Her force calculation results compared well with the measured forces, but were subject to error because she assumed steady flow, constant pressure, and conservation of mass in two-dimensions while applying the integral momentum equation.

The purpose of this paper is to investigate the behavior of three-dimensional flapping foils by building upon the work already done on two-dimensional flapping foils and cylinders.

II. Experimental Setup

A. Mechanical Design of the Actuator Module

The flapping foil actuator module used in the experiments was designed for use on an autonomous underwater vehicle, and was modified for use in the MIT Marine Hydrodynamics Water Tunnel. The module is made up of a waterproof box that contains two DC drive motors and the motor control electronics.

Figure 1 shows a solid model drawing of the actuator. The waterproof box is $22cm$ square by $61cm$ long, and is made

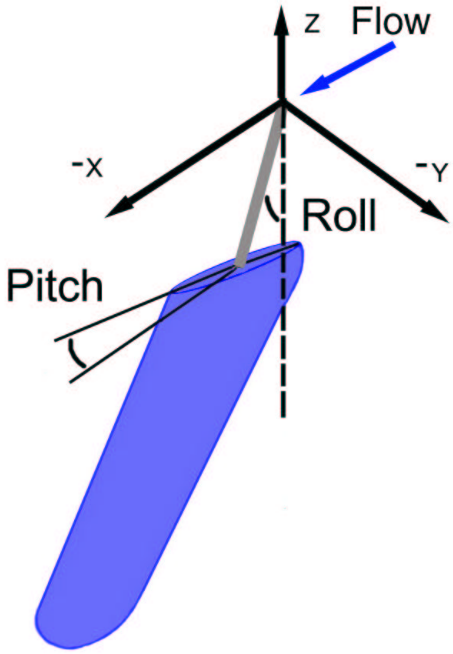

Fig. 2. Sketch of a three-dimensional flapping foil

of $19mm$ clear lexan. The box has a removable side access panel and a slot for the foil shaft,

The pitch motor assembly is made up of a 24 V, 1.8 Amp DC brush motor (Litton Polyscientific, Blacksburg VA), two bearings, and anti-backlash gears. The entire pitch assembly is mounted to an aluminum plate. The aluminum plate is supported by a a double-roller taper bearing on one side, and by a coupling to the roll motor shaft on the other side. The roll motor is a 24 V, 8.2 Amp DC brush motor also made by Litton Polyscientific.

The slot in the lexan box for the foil shaft is sealed with a large, corrugated, rubber bellows. The corrugation of the bellows allows the foil to roll while an O-ring shaft seal at the center of the bellows allows the foil to pitch.

The foil used for all experiments has a linearly tapered trailing edge and straight leading edge. It has a NACA 0012 section, an average chord of 5.5 cm and a span of 24.3 cm. The maximum chord is 7.5 cm at the root and tapers to 3.5 cm at the rounded tip. It was constructed using a stainless steel triangular skeleton and polyurethane plastic in a mold. A $6.4mm$ diameter stainless rod welded to the skeleton was inserted in the mold at the approximate $1/4$ chord position. The foil was spray painted black to absorb laser light for safety reasons and sanded for a smooth finish. In Figure 2, the foil rolls about the x-axis and pitches about the z-axis while the uniform inflow is in the +x direction.

B. Water Tunnel Installation

All experiments described in this paper were conducted in the MIT Department of Ocean Engineering Water Tunnel, a two-storey closed-loop water tunnel. Flow through the tunnel is driven by an impeller located under the test section. The test section is made up of four clear, removeable windows that are 0.50 meters wide by 1.5 meters in length. Figure 3 shows the test section of the tunnel with the flapping foil installed. Free stream turbulence intensity as a function of tunnel speed was measured previously in the empty test section using hot wire anemometry, showing a level of 1% for the conditions of these tests.

Figure 4 shows a view of the actuator module disassembled in the water tunnel. The module is installed through the top window of the test section and hangs from a three-axis dynamometer. The dynamometer holds the foil actuator via a shaft attached to the module box. A three-piece aluminum housing was constructed to fit between the top of the tunnel test section and the dynomometer to surround the module. A fairing was also constructed using wood and waterproof sealant to minimize flow interaction with the foil module. Hydrodynamic forces on the foil shaft and bottom of the actuator module were assumed to be negligible due to the shielding of the fairing.

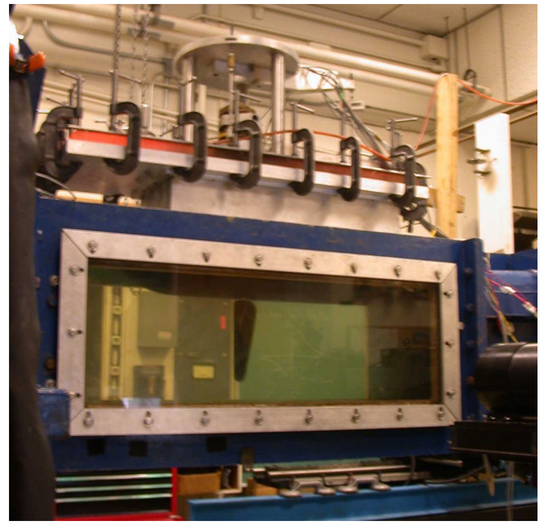

Fig. 3. Module Housing Assembly Installed in the Water Tunnel

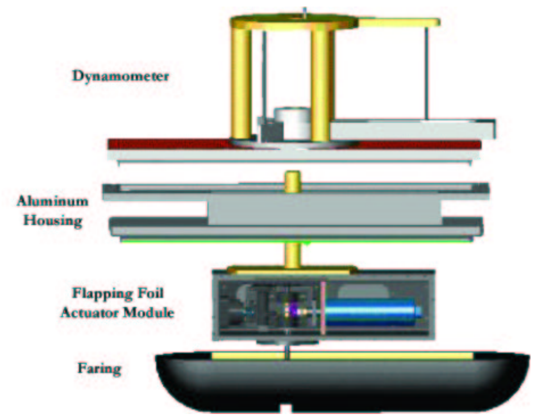

Fig. 4. Module Housing Assembly

C. Actuator Electronics and Data Collection

The electronics and data collection system is made up of a motor control card and amplifier inside the module and two PCs outside of the module that command the foil and collect data.

Communication and power reaches the interior electronics through two waterproof Impulse Connectors (Impulse Enterprises, San Diego CA). Power is supplied by a 24V power supply. A DC converter inside the module distributes power to the electronics and motors.

Control of the motors was accomplished using a Galil, two-axis, PID motion control card, which received commands from the control PC. The control PC runs a C++ interface code that commands the motors, records encoder feedback, and creates a square wave pulse signal that switches when the roll angle crosses zero. This pulse signal is used to sync the dynamometer records with the position records and to sync the DPIV system with the foil movement.

Force measurements were recorded on a separate PC with a data acquisition card. The card collected and recorded the pulse signal, lift force, and thrust force at 1000 Hz.

All signals were processed and filtered in Matlab. A spectral analysis of the force signals was performed and it was found that the signals had peaks between 10 and 13 Hz due to structural vibrations of the water tunnel. All force signals were filtered to cutoff frequencies above 8 Hz.

D. DPIV Setup

The digital particle image velocimetry, DPIV, system was set up externally to the test section of the water tunnel to analyze the flow around the foil. Unlike other particle flow visualization methods, DPIV allows the measurement of an entire instantaneous 2-D or 3-D velocity particle field.

The DPIV system (LaVision Inc, Goettingen Germany) shines a horizontal pulsed laser sheet through the acrylic side walls of the test section, and records the illuminated sheet of particles with an upward-looking camera located below the test section. To illuminate a horizontal plane, the laser beam (a 120 mJ/pulse ND:Yag laser operating at 532 nm) is focused and then fanned to form a thin 2-D sheet of light. Both the camera and laser were mounted on a traverse so that they could be precisely positioned.

For the flapping foil experiments, the pulse signal from the foil module was used to trigger the laser system. The system was set to take twelve pairs of images during one period of the foil's motion.

III. Experimental Methods

The flapping foil was tested over a range of actuation frequencies and amplitudes. Streamwise force, (thrust), and transverse force (lift) measurements were taken for symmetrically flapping and pitch biased foils. Extensive DPIV data was also obtained for one case of the pitch biased foil.

A. Force Measurement Methods

The non-dimensional parameters of heave amplitude ($h_{0.7}/c$), Strouhal number (St), and maximum angle of attack (α_{max}) define the foil motion for all tests.

The non-dimensional heave amplitude is defined as:

$$h_{0.7}/c = R_{0.7}\phi_o/c, \qquad (1)$$

where $R_{0.7}$ is the distance in meters from the center of rotation to the 0.7 span of the foil, ϕ_o is the roll amplitude in radians, and c is the average chord of the foil. Heave amplitude was defined at the 0.7 span because this is approximately the center of force for a three-dimensional foil.

The Strouhal number for the three dimensional flapping foil is defined as:

$$St = \frac{2h_{0.7}f}{U}, \qquad (2)$$

where f is the flapping frequency in Hz, and U is the flow velocity in meters/second. $2h_{0.7}$ was chosen as an an estimate of the width of the foil wake at the mid-span.

The maximum angle of attack is the largest angle that the pitching foil makes with the net incoming flow, where the net incoming flow is a vector combination of the tunnel flow and the apparent flow from the angular roll velocity.

The maximum angle of attack, calculated at $R_{0.7}$, over one period, T, is defined as:

$$\alpha_{max} = max\{\alpha(t)\} \qquad (3)$$

$$\alpha(t) = \arctan(R_{0.7}\phi_o\omega\cos(\omega t)/U) - \theta_o\sin(\omega t + \pi/2), \qquad (4)$$

where θ_o is the pitch amplitude in radians and ω is the angular flapping frequency. Also, a phase angle between pitch and roll of $\pi/2$ is assumed. The derivation of this equation is described in detail by Harness [8].

To reach the desired St, α_{max}, and h_o/c for a given test, the flapping frequency, roll amplitude, pitch amplitude, and tunnel flow speed were adjusted. To reach the higher Strouhal numbers, the tunnel flow speed had to be lowered to its lowest stable speed of $U = 0.40\ m/s$. The flow rate was monitored with the Tunnel's LDV system to stay within $0.01\ m/s$ of the desired rate.

B. DPIV Methods

For the DPIV analysis, the foil was actuated at a Strouhal number of 0.5, an h_o/c of 1.5, and a pitch bias angle of $19°$. At these actuation parameters the foil produces almost no thrust, but has a mean lift coefficient of 1.8.

The DPIV system was used to record the two-dimensional flow at six spanwise locations along the foil. At each of these spanwise locations the DPIV system was triggered to take thirty pairs of images while the foil was at twelve different roll positions. These twelve roll positions made up an entire period of motion.

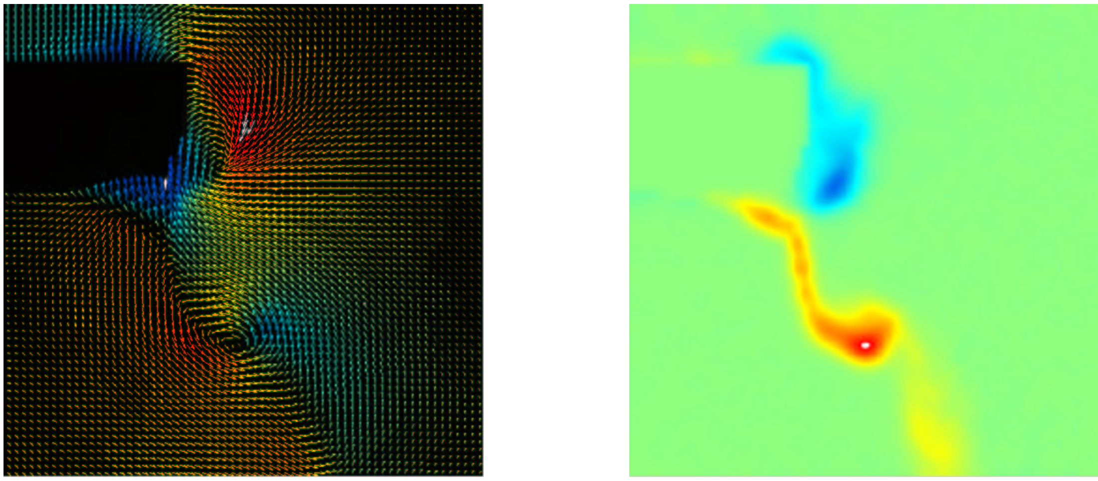

(a) velocity (b) vorticity

Fig. 5. Velocity and Vorticity Plots at the 0.7 Radius

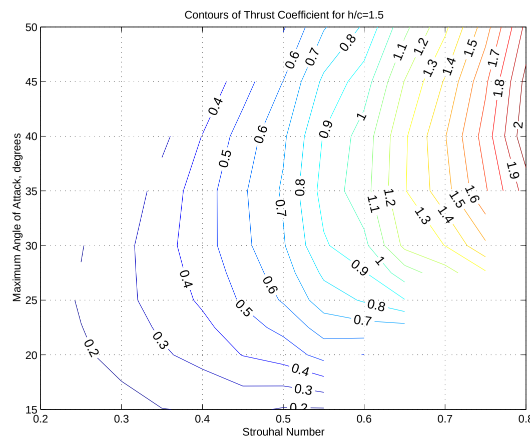

Fig. 6. Contours of thrust coefficient for $h_{0.7}/c = 1.5$

In post-processing, the pairs of images were analyzed to make vector plots of the flow velocities Figure 5(a). The thirty vector plots for each roll position were averaged to smooth out any errors. The computational methods used are described and analyzed by Willert and Gharib [9] as well as Adrian [10]. The vorticity of each velocity field was also computed for a clearer picture of the flow behavior, Figure 5(b).

The foil in the laser sheet casts a shadow of unilluminated particles. To get complete velocity fields and vorticity plots, the images of opposite roll angles were flipped and combined as shown if Figure 10.

IV. Results and Discussion

A. Symmetric Motion

A symmetrically flapping foil produces a positive average thrust force while the lift force averages to zero.

The average thrust force is non dimensionalized as:

$$C_T = \frac{\overline{F}}{\frac{1}{2}\rho U^2 cs}, \tag{5}$$

where $\overline{F}$ is the thrust force averaged over 50 cycles of motion, ρ is the density of water, c is the average foil chord, and s is the foil span.

In Figure 6 the results of experiments conducted at a roll amplitude of $h_{0.7}/c = 1.5$ are shown. Two runs were conducted at each point to validate repeatability. Data was collected at every thrust producing combination of α_{max} and Strouhal number allowed by the actuator. No data was collected at low α_{max} and high Strouhal number because a high pitch amplitude would be required to meet these conditions. High pitch amplitudes at high frequencies would have damaged the actuator.

Figure 6 shows that, in every case, the thrust coefficient increases with Strouhal number. At low α_{max}, the transition from drag to thrust occurs around a calculated Strouhal number of 0.2. However, at high α_{max}, the transition to thrust does not occur until a Strouhal number of 0.4.

The maximum thrust coefficient of 2.07 occurs at 40 degrees maximum angle of attack and Strouhal number of 0.80. This thrust coefficient is normalized by the planform area of the foil, while the thrust coefficients of traditional rotary propellers are normalized by their swept area. Normalizing the foil's thrust coefficient by swept area instead of planform area lowers it to 0.63. Rotary propellers used on passenger ships and high speed naval vessels often operate at a thrust coefficient of 0.63 [11].

B. Pitch-Biased Flapping

A pitch-biased flapping foil has a static bias added to the sinusoidally oscillating pitch angle. α_{max} is increased by the bias angle while the minimum angle is reduced.

Pitch biased experiments were conducted in the parameter space of good thrust producing runs from the propulsion results. A maximum angle of attack of $40°$ was tested for

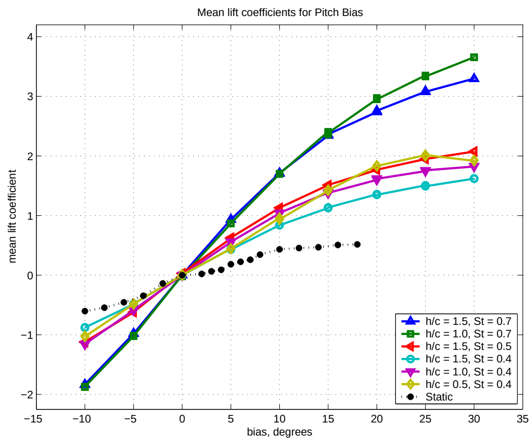

Fig. 7. Mean lift coefficients for Bias Tests

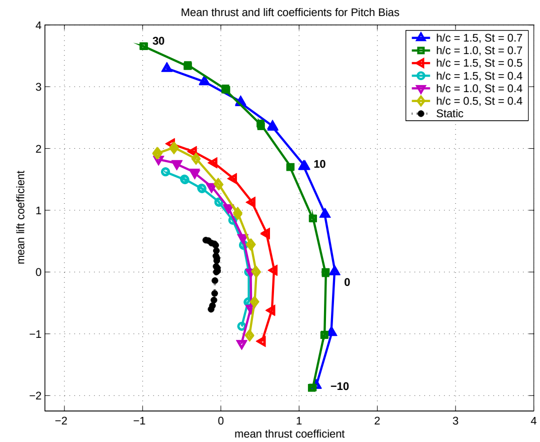

Fig. 9. Mean thrust and lift coefficients for Bias Tests

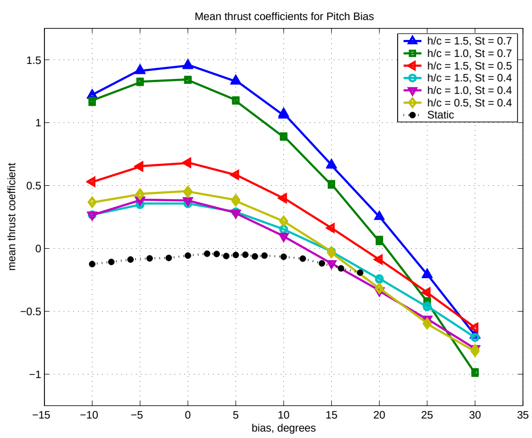

Fig. 8. Mean thrust coefficients for Bias Tests

Strouhal numbers 0.4 and 0.7 for $h_{0.7}/c = 1.0$ and 1.5, with one additional experiment at $h_{0.7}/c = 0.5$ for a Strouhal number of 0.4. Pitch biases ranged from -10 to 30 in increments of $5°$. Negative pitch bias was added to show that the lift forces are symmetric for positive and negative bias. The lift force is non-dimensionalized into the lift coefficient, C_L in the same way that the thrust force is non-dimensionalized into C_T.

Figure 7 shows the mean lift coefficients for a $40°$ maximum angle of attack. They are plotted with the lift results for a static foil. Very large values of lift are obtained for the flapping cases. The lift coefficient seems to be very much dependent on the Strouhal number while the effect of $h_{0.7}/c$ appears to be small. However, in both the lower Strouhal number and higher Strouhal number comparisons, the runs with the lowest $h_{0.7}/c$ value had slightly higher mean lift coefficients. This ability to generate high lift with low amplitude flapping is noteworthy because smaller motions present an easier mechanical design.

Figure 8 plots the mean thrust coefficients as a function of bias angle for two different Strouhal numbers and three different $h_{0.7}/c$ values. Comparing this plot to Figure 6 shows that adding pitch bias always decreases the thrust coefficient. At $30°$ bias angle, the thrust coefficient appears to be almost independent of the Strouhal number. Also, the thrust coefficient becomes negative at $15°$ bias for the lower Strouhal number cases, and $20°$ bias for the higher Strouhal number cases. Finally, it is important to note that small bias angles still produce useful amounts of thrust, especially for high Strouhal number. As is true with lift, the effect on thrust of $h_{0.7}/c$ appears to be small.

The mean lift and thrust coefficients are plotted together in Figure 9. The horizontal axis represents C_T and the vertical axis C_L. A few bias angles are labelled in the figure. The transition from thrust to drag producing motions occur for a bias angle between $15°$ to $25°$. Since the flapping foil is used for both propulsion and maneuvering, the magnitude and direction of the forces produced can be deduced from this plot of their components. Components of negative thrust with high lift represent parameters would provide a maneuvering and braking force. Components of thrust and moderate values of lift would provide a maneuvering and propulsion force.

C. DPIV

Figure 10 shows a schematic of the vortices shed from the foil during a period of motion.

As the foil passes the zero-roll position, (d), it sheds a positive leading edge vortex and a negative trailing edge vortex. Due to the pitch-biasing, during the second half of its cycle (g-l) it only produces a small, negative leading edge vortex with no significant trailing edge vortex. The dominant characteristic of this vortex wake is the dissimilarity to that of a symmetric flapping motion, where a regular reverse Karman vortex street is created, with two equal pairs of vortices shed. The reverse Karman vortex street produces only a net thrust, while this vortex wake produces only a net lift.

Along with a qualitative understanding of the vortex patterns, the DPIV images at the six spans of the foil can provide quantitative values for the forces acting on the foil. Both the integral momentum equation and Lighthill's moment of vorticity equation can potentially be used for force calculations.

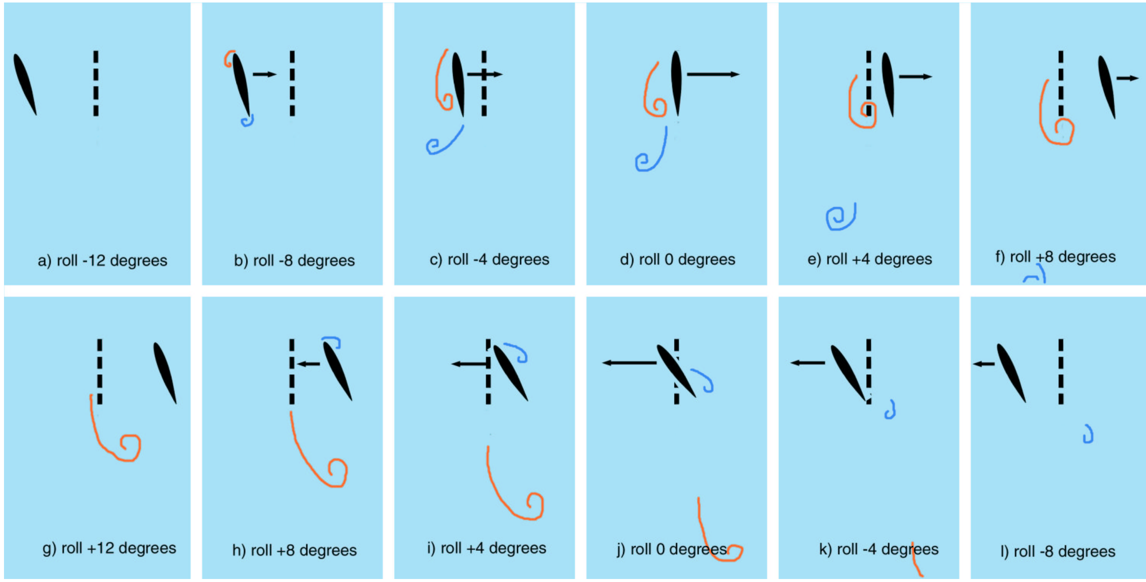

Fig. 10. Vorticity at $R_{0.7}$ for a period of motion. The dashed line represents the zero-roll position of the foil, and the arrow represents the magnitude and direction of the foil's velocity.

V. Conclusion

The results of the force analysis confirm that three-dimensional flapping foils may be a viable alternative to traditional propulsors. The flapping foil module's ability to produce combinations of high thrust and lift allow for force vectoring in the plane perpendicular to the pitch axis. Vehicles using these modules would excel at both cruising and maneuvering.

The results of the ongoing DPIV analysis will provide accurate force measurements at each span and an understanding of the vorticity patterns. This knowledge will allow for the optimization of flapping foil shape and movement and could also be applied to the development of propellers with rapidly variable pitch. In future tests, to capture as much of the velocity field as possible, a second camera will take images of the wake, and dual laser sheets will be used to eliminate the shadowed region.

Future work into three-dimensional flapping foils will involve a more comprehensive force and DPIV study combined with an efficiency analysis.

Acknowledgment

The authors acknowledge with gratitude financial support by the MIT Sea Grant Program and the Office of Naval Research STTR Contract N0014-02-M-0219, monitored by Dr. P. Bandyopadhyay.

References

[1] D. Read, "Oscillating foils for propulsion and maneuvering of ships and underwater vehicles," Master of Science in Naval Architecture and Marine Engineering, Massachusetts Institute of Technology, MA, February 1999.

[2] N. Kato, "Control performance in horizontal plan of fish robot with mechanical pectoral fins," *IEEE Journal of Oceanic Engieering*, vol. 25, 2000.

[3] E. Obasaju, "A study of forces, circulation, and vortex patterns around a circular cylinder in oscillating flow," *Journal of Fluid Mechanics*, vol. 196, pp. 467–494, 1987.

[4] F. Noca, "A comparison of methods for evaluating time dependent fluid dynamic forces on bodies, using only velocity fields and their derivatives," *Journal of Fluids and Structures*, vol. 13, pp. 551–578, 1999.

[5] M. Unal and J. Lin, "Force prediction by piv imaging: A momentum-based approach," *Journal of Fluids and Structures*, vol. 11, pp. 965–971, 1997.

[6] J. Lin and D. Rockwell, "Force identification by vorticity fields: Techniques based on flow imaging," *Journal of Fluids and Structures*, vol. 10, pp. 663–668, 1996.

[7] J. Anderson, "Vorticity control for efficient propulsion," PhD Thesis in Oceanographic Engineering, Massachusetts Institute of Technology, MA, February 1996.

[8] M. Flores, "Flapping motion of a three dimensional foil for propulsion and maneuvering of underwater vehicles," Master of Science in Ocean Engineering, Massachusetts Institute of Technology, MA, May 2003.

[9] C. Willert and M. Gharib, "Digital particle image velocimetry," *Exp. Fluids*, vol. 10, pp. 181–193, 1991.

[10] R. Adrian, "Particle imagining techniques for experimental fluid mechanics," *Ann. Rev. Fluid Mech.*, vol. 23, pp. 261–302, 1991.

[11] J. Breslin and P. Anderson, *Hydrodynamics of Ship Propellers*. Cambridge: Cambridge University Press, 1994.